Comparison of instrumentally measured temperature with other instrumentally measured or observed geophysical quantities.

Mikhail Kovalyov

February 27, 2022

Abstract. In this review, we demonstrate a striking similarity between instrumentally measured temperature, the speed of the magnetic North Pole as a proxy for the changes in the Earth's magnetic field, seismic activity, and UFO sightings as a proxy for energy transfer between near-Earth space and the Earth's atmosphere. New research (some as recent as 2021) points towards the Van Allen Belts as the main contributor to global warming.

Key words. Global warming, Earth's magnetic field, Van Allen Belts, undetermined areal phenomena.

In this review, we demonstrate a striking similarity between instrumentally measured temperature, the speed of the magnetic North Pole as a proxy for the Earth's magnetic field, seismic activity, and UFO sightings as a proxy for energy transfer between near-Earth space and the Earth's atmosphere. While many a pundit stridently clamor that UFOs are indicative of extraterrestrial aliens, we will show that UFOs are but a facet in a large-scale natural phenomenon of terrestrial origin. The similarity between global temperature and several other distinct and seemingly unrelated natural phenomena points towards the natural origin of global warming, which goes contrary to the current consensus that global warming is caused by the greenhouse effect resulting from increased levels of CO_2.

As a reference point for global temperature we use Figure 1, showing measurements by six reputable agencies. Figure 2 shows CO_2 concentration and emission, it bears no resemblance to and shows no correlation with the graph in Figure 1, other than that CO_2 concentration and the graph in Figure 1 increased in $1980 - 2020$. Yet, as Figure 3 demonstrates, there is a remarkable similarity between temperature and the speed of the magnetic North Pole in $1900 - 2010$; the similarity clearly extends to the graph in Figure 1.

In Figure 3 all but one changes in the speed of the magnetic North Pole precede corresponding

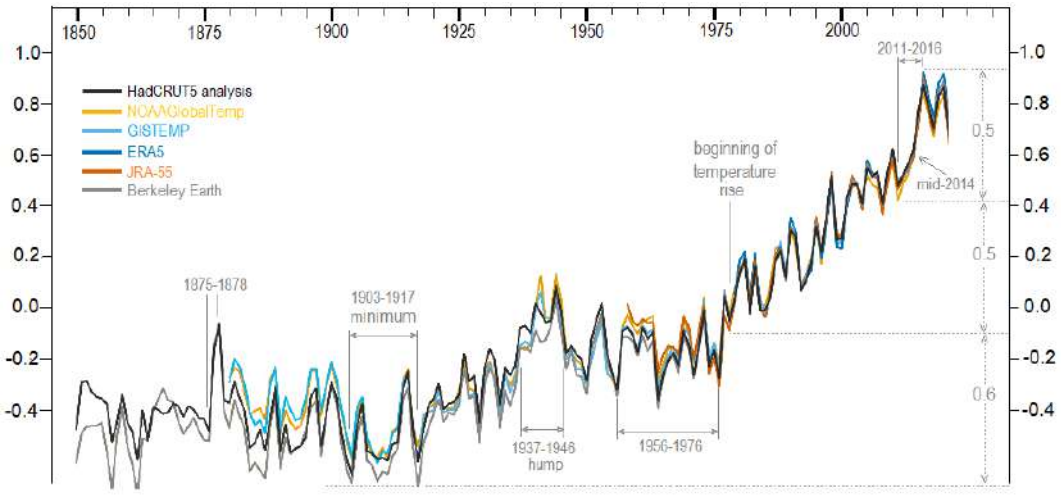

Figure 1: Annual global temperature anomalies in ^oC in 1900 – 2020 by six agencies, [1]. The largest known uninterrupted increase in global temperature was in 2011 – 2016.

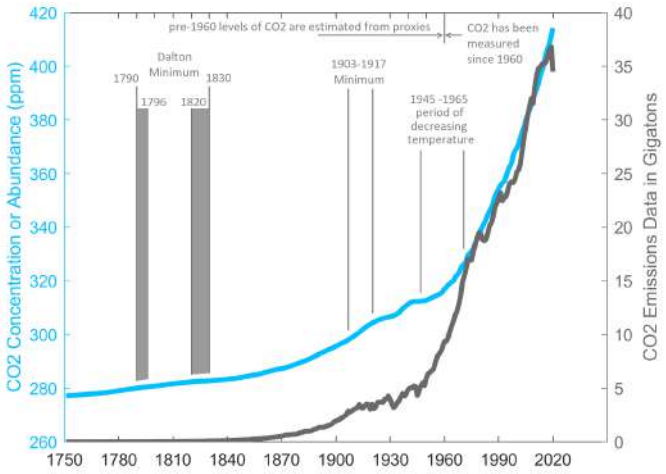

Figure 2: CO_2 concentration and emission. The original graph was produced and kindly emailed to the author of this paper by Dr. Howard Diamond, Climate Science Program Manager, NOAA. Comments were added by the author of this paper. The graph of CO_2 concentration bears no resemblance to and shows no correlation with the graphs in Figures 1, other than that CO_2 concentration and the graphs in Figures 1 increased in 1980 – 2020. Nor is the 1903 – 1917 temperature minimum reflected in the CO_2 graph in any way; as a matter of fact, the rate of increase of the CO_2 graph accelerated during the 1903 – 1917 temperature minimum. Even more bemusing is that the 1945 – 1965 period of decreasing temperature in Figure 1 seems to have coexisted with the rising levels of CO_2 shown above. The definition of the Dalton Minimum varies between 1790 – 1830 and 1796 – 1820, both options are shown; yet, whichever time window is chosen, the graph of CO_2 does not give even the tiniest hint of a temperature minimum.

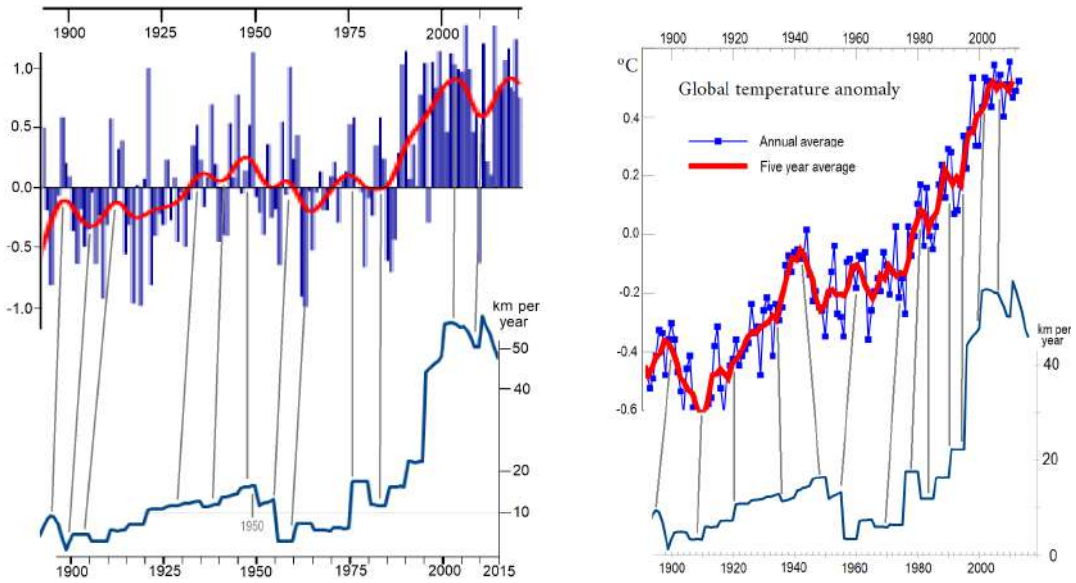

Figure 3: The top graph in the left pane shows mean Central England temperature annual anomalies in 1659 – 2010 in blue and its average in red, numerical data is from Met Office, [2]. The top graph in the right pane shows the instrumental record of global average temperatures compiled by NASA's Goddard Institute for Space Studies, [3]; the zero is the mean temperature in 1961-1990. The bottom graphs show the speed of the magnetic North Pole, constructed from NOAA's data and scaled to fit the top graphs, [4]. The gray lines indicate how the points on the graph of the magnetic North Pole's speed correspond to the points on the temperature graphs.

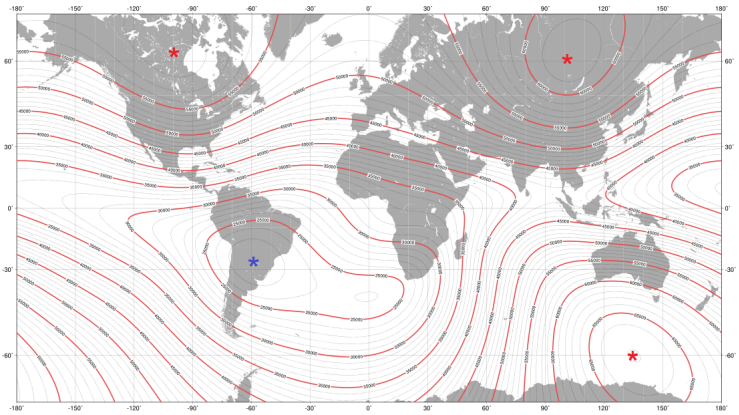

Figure 4: Total intensity of the Earth's magnetic field on 2020/1/1, [5]. The absolute minimum $22\,231.9\,nT$ at $26.1^{\circ}S, 59.2^{\circ}W$ is marked by a blue asterisk. The three global maxima are marked by red asterisks: 1) North-Eastern maximum $61\,746.1\,nT$ at $61.4^{\circ}N, 102.4^{\circ}E$, 2) North-Western maximum $58\,632.3\,nT$ at $62.4^{\circ}N, 99.0^{\circ}W$; 3) Southern maximum $66\,991.6\,nT$ at $60.0^{\circ}S, 135.4^{\circ}E$. NOAA's model shows that the relative contribution of the North-Western maximum was larger than that of the North-Eastern maximum before 1948/11/27, while it was smaller after 1948/11/27, [5]. In reality, the tussle for superiority between the two maxima must have lasted for years with baton changing hands more than once. On 2020/1/1, the North-Eastern maximum was ≈ 59 km from the epicenter of the Tunguska explosion at $60.917^{\circ}N, 101.95^{\circ}E$.

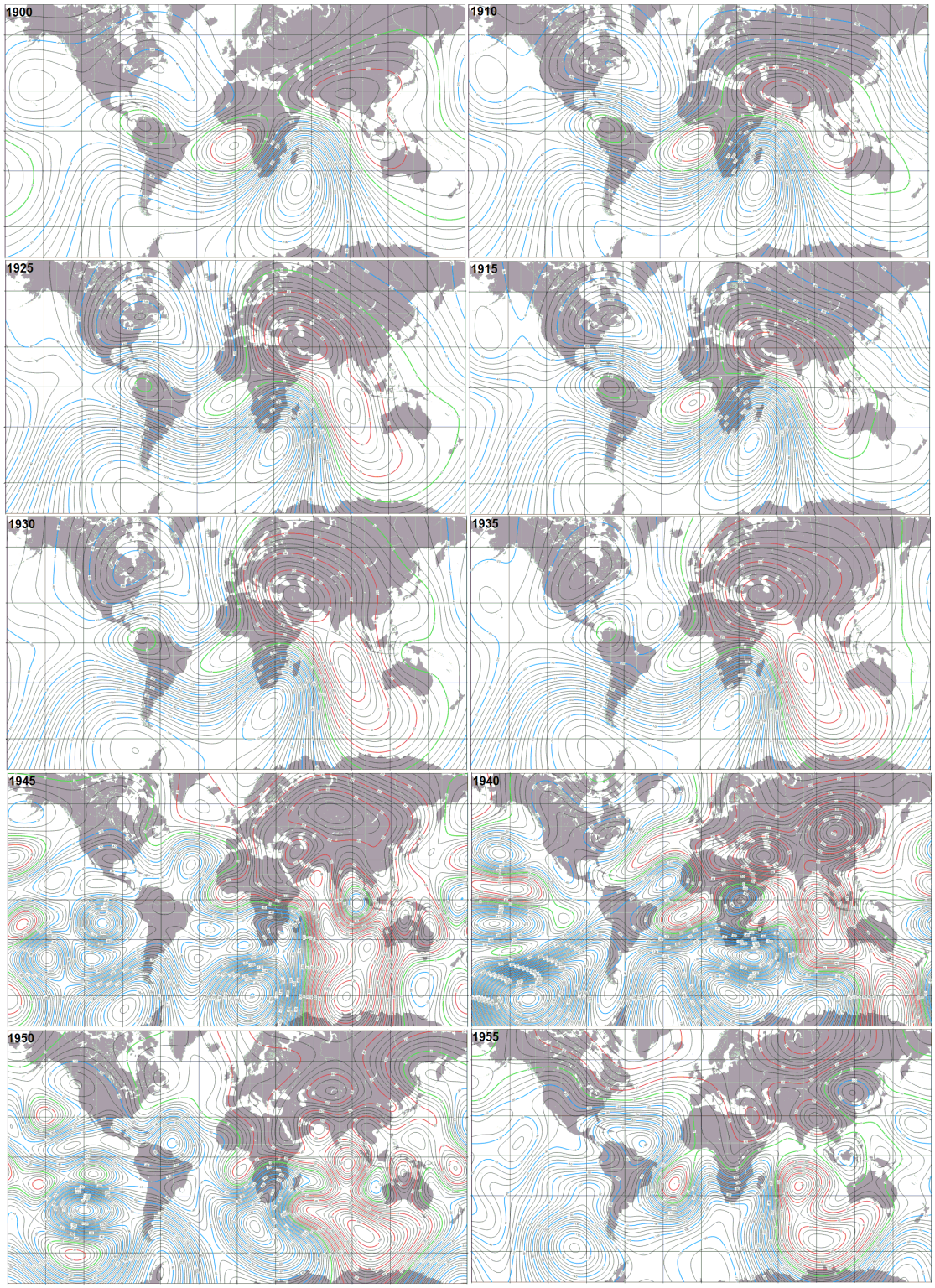
1900
1910
1925
1915
1930
1935
1945
1940
1950
1955

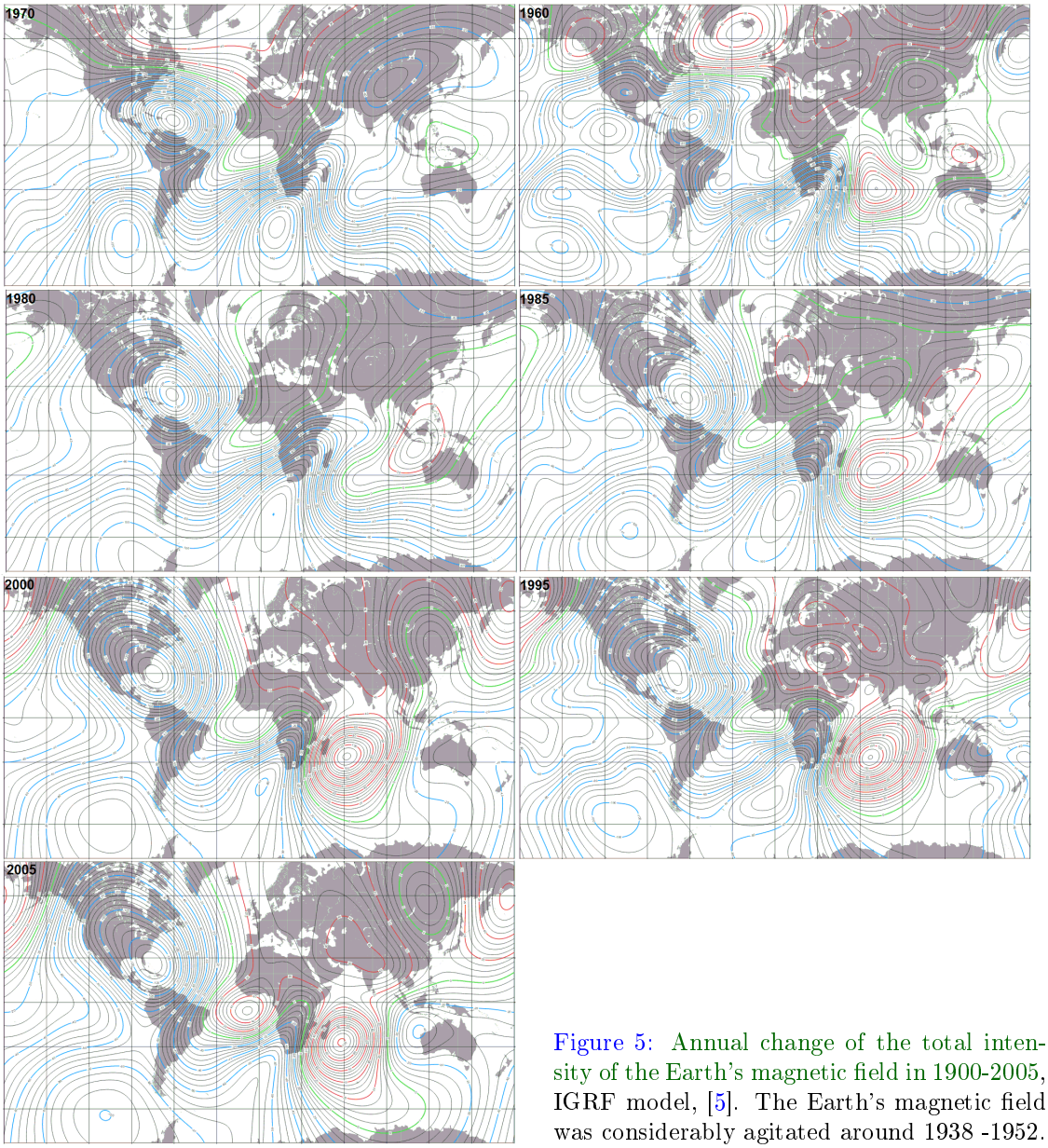

Figure 5: Annual change of the total intensity of the Earth's magnetic field in 1900-2005, IGRF model, [5]. The Earth's magnetic field was considerably agitated around 1938 -1952.

changes in temperature; the only exception being the 1945 – 1950 maximum in the speed of the magnetic North Pole somewhat lagging the corresponding temperature maximum. Although it might be attributed to the absence of actual measurements of the magnetic North Pole in 1905 – 1947 and 1949 – 1962, [6], the actual reason is most likely the tussle for superiority explained in Figure 4. It resulted in 1) the agitation of the Earth magnetic field illustrated by Figure 5;

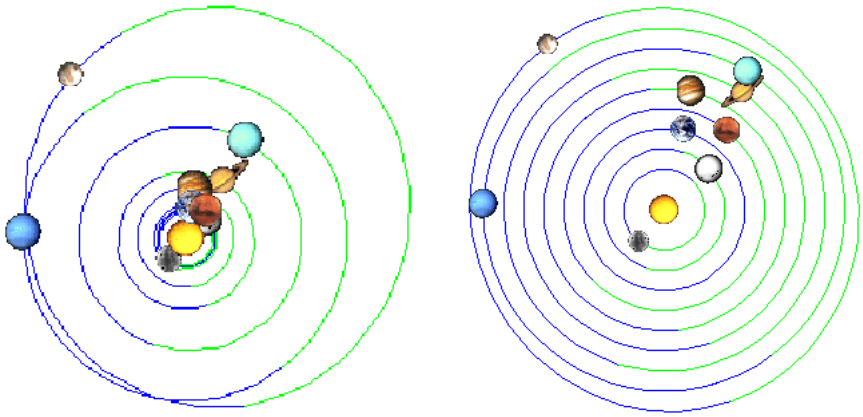

Figure 6: Solar system on 1941/12/8. On the left, orbits are shown in real configuration; on the right, orbits are shown as equidistant circles, [7]. With 1941/12/8 Jupiter opposition, 1941/11/17 Saturn opposition, 1941/11/21 Uranus opposition, 1941/11/10 Mars opposition, and 1942/2/2 Venus conjunction with Sun, 96.1% of planetary mass of the Solar system lined up along a single line; of that Jupiter makes 71.2%, Saturn 21.3%, Uranus 3.3%, Earth 0.2%, and Venus 0.2%.

2) an increase in the speed of the magnetic North Pole, attaining in 1950 the highest value over 1590 – 1974; 3) the 1938 – 1946 increase in earthquake activity with thirteen magnitude $\geqslant 8.0$ earthquakes or 1.44 earthquakes per year, for comparison, 1900 – 1999 saw 70 such earthquakes or 0.7 earthquakes per year, [9]; 4) the 1937 – 1946 temperature maximum. It was also accompanied by an unusual increase in the number of unrecognized aerial phenomena, often referred to as foo fighters, unsuccessfully investigated by the Robertson Panel, Projects Sign, Grudge, Blue Book; and 28 unusually powerful auroras on 1936/6/10, 1936/6/19, 1937/2/28, 1937/4/28, 1937/8/3, 1938/1/25 Fatima geomagnetic storm, 1940/3/25, 1940/4/3, 1941/1/18, 1941/7/6, 1941/9/18, 1942/6/27, 1943/9/4, 1944/10/15, 1944/12/17, 1946/2/3, 1946/3/24, 1946/4/8, 1946/7/26, 1947/3/8, 1947/7/19, 1947/8/27, 1948/3/16, 1949/1/27, 1950/2/21, 1950/8/20, 1951/7/2, 1951/9/23, [10].

Figure 6 shows an unusual configuration of the Solar System on 1941/1/2/8 with six out of seven most massive planets aligned along a single line, somewhat similar but less precise congregations occurred during 1937 – 1946. Such arrangements were bound to increase solar emissions in the direction of the planets, hence it is likely that the configuration contributed to an already-building global temperature maximum and the global temperature maximum appearing several years before the 1950 maximum in the speed of the magnetic North Pole. A minor temperature increase around 1976 might have been caused by a congregation of Jupiter, Earth, Venus and Mer-

cury within a small cone in the Solar System due to the 1976/5/17 Jupiter opposition, 1976/7/14 Venus conjunction, 1976/6/16 Mercury conjunction; a somewhat similar congregation occurred in 1977.

In 2010 – 2016, the influence of the Earth's magnetic field on temperature was superseded by that of tidal forces. On 2010/1/30, 2011/3/19, 2012/5/6, 2013/6/23, 2014/8/10, 2015/9/28, and 2016/11/14, Full Moon and perigee came within, correspondingly, 165, 59, 2, 23, 27, 65, and 150 minutes of each other synchronizing the increases in tidal pull due to Full Moon and perigee, [11]. Never in the known history have Full Moon and perigee been merely 2 minutes apart as on 2012/5/6; nor have they been $\leqslant 65$ minutes apart for 5 years in a row or $\leqslant 165$ minutes apart for seven years in a row. The increases in tidal force due to the synchronization of Full Moon and perigee were further amplified by the 2010/1/29, 2012/5/7, 2013/6/20 lunar nodes, and 2015/9/27 eclipse. We shall refer to a pair of a Full Moon and a perigee that come within 11 hours of each other as *Full Moon-perigee*, *New Moon-perigee* is defined similarly. Full Moon-perigees recur on average every 412 - 413 days, and so do New Moon-perigees. On 2010/9/6, 2011/10/26, 2012/12/12, 2014/1/1, 2015/2/19, 2016/4/7 New Moon and perigee came within 9 hours of each other, which by itself is nothing to write home about, but the increase in tidal force was amplified by the 2010/9/4, 2011/10/29, 2012/12/11, 2015/2/21, 2016/4/5 lunar nodes, 2013/1/2, 2014/1/4 perihelia, 2010/9/21, 2011/10/29, 2012/12/3, 2014/1/5, 2015/2/6 Jupiter oppositions, 2010/9/21 Uranus opposition, 2014/1/11 Venus-Sun conjunction, [8].

Although the increase in tidal force was rather small, it nevertheless brought the tidal force close to an all-time high, and must have contributed to terrestrial and near-terrestrial events: 1) a never-before-seen alignment of magnitude $\geqslant 7.9$ earthquakes with Full Moon-perigees shown in Table 1; 2) one of the only two known cases of three magnitude $\geqslant 8.5$ earthquakes striking three years in a row on 2010/2/27, 2011/3/11, 2012/4/11, accompanied by the 2011/6/30-4 VEI=5 eruption of Puyehue, only once before three powerful earthquakes struck three years in a row on 1963/10/13, 1964/3/28, 1965/2/4, accompanied by the 1963/3/18 VEI=5 eruption of Agung, [9, 14]; 3) the only known appearance of the third Van Allen Belt, followed by waxing and waning of the Belts, obliteration of the outer and middle Belts, and final recovery of the known Belts' structure, [15]; 4) the only observed space hurricane detected on 2014/8/20, [16]; 5) the all-time high speed of the magnetic North Pole, [4]; and 6) an uninterrupted temperature rise in Figure 1.

Full Moon-perigees in 2010/1/1 – 2016/12/31	days between	Magnitude $\geqslant$ 7.9 earthquakes in 2010/1/1 – 2016/12/31		
2016/11/14	33	2016/12/17	M=7.9	Papua New Guinea
2015/9/28	12	2015/9/16	M=8.3	Alaska
2014/8/10	48	2014/6/23	M=7.9	Alaska
none		2014/4/1	M=8.2	Chile
2013/6/23	30	2013/5/24	M=8.3	Russia
none		2013/2/6	M=8.0	Solomon Islands
2012/5/6	25	2012/4/11	M=8.2 aftershock	
2012/5/6	25	2012/4/11	M=8.6	Indonesia
2011/3/19	8	2011/3/11	M=7.9 aftershock	
2011/3/19	8	2011/3/11	M=9.1	Japan
2010/1/30	28	2010/2/27	M=8.8	Chile

Table 1: Alignment of magnitude $\geqslant$ 7.9 earthquakes, [9], with Full Moon-perigees, [11]. Full Moon-perigees recur approximately every 412 - 413 days. In 2010/1/1 – 2017/1/1, $\approx 91\%$ of M $\geqslant$ 7.9 earthquakes struck within 48 days of a Full Moon-perigee. If earthquakes struck randomly, only $\approx \frac{96}{412} \times 11 \leqslant 3$ earthquakes would be expected to strike within 48 days of a Full Moon-perigee; not all 9. The 2014/4/1 earthquake was not within 48 days of a Full Moon-perigee; however, it coincided with the 2014/3/30 – 2014/4/1 New Moon and lunar node and followed a rather unusual coalescence of the 2014/1/1 New Moon-perigee, 2014/1/4 perihelion, 2014/1/5 Jupiter opposition, 2014/1/11 Venus-Sun conjunction, and 2013/12/29 Mercury-Sun conjunction, all resulting in increased tidal force.

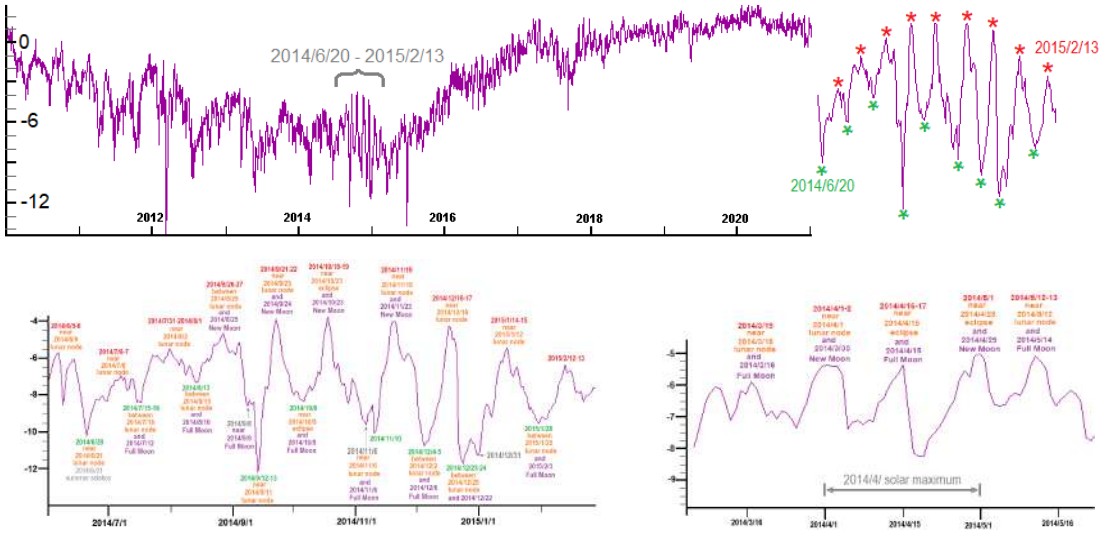

Figure 7: Cosmic rays variations, daily resolution, [12]. It shows rather unusual undulations in 2014/6/20−2015/2/13 with the maxima/minima marked correspondingly by red/green. Maxima/minima are close to lunar nodes, maxima are close to New Moon, minima are close to Full Moon, [11]. The undulations were preceded by the 2014/3/15 – 2014/5/15 14-day recurrence of maxima shown in the bottom right pane. Although 27-day variability in cosmic rays is well-known, it has never been so strongly exhibited; nor is it well-understood for as [13] points out "existing theoretical models are not able to adequately reproduce characteristics of 27-day variations in the particle flux".

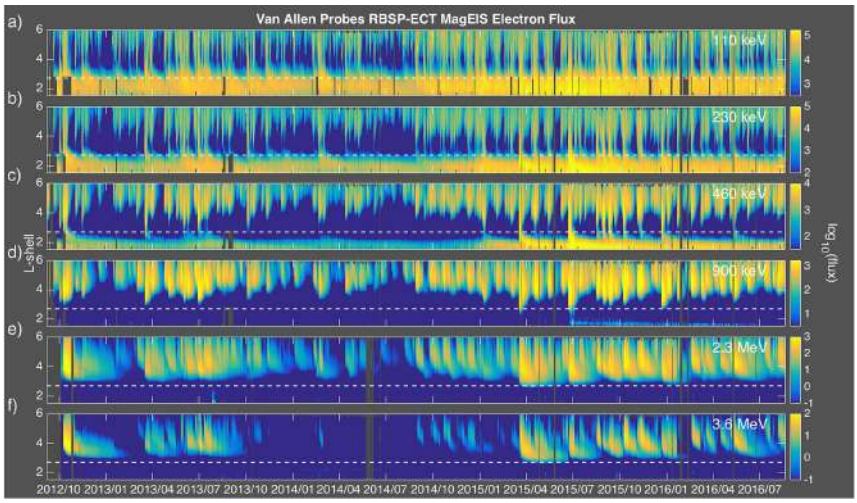

Figure 8: Electron differential fluxes in the inner Van Allen Belt from the MagEIS instruments on the Van Allen Probes spacecraft, [18]. Flux here is in units of $\#/(cm^2 ssr KeV)$. Data from both RBSP A and B are shown in color (log10(flux)) binned in time and L shell during the period from launch in September 2012 through February 2016. From top to bottom, each plot shows results from a different energy channel, as labeled in the top right of each plot. The graph shows flux drop for low L around 2013/10/ – 2015/3/.

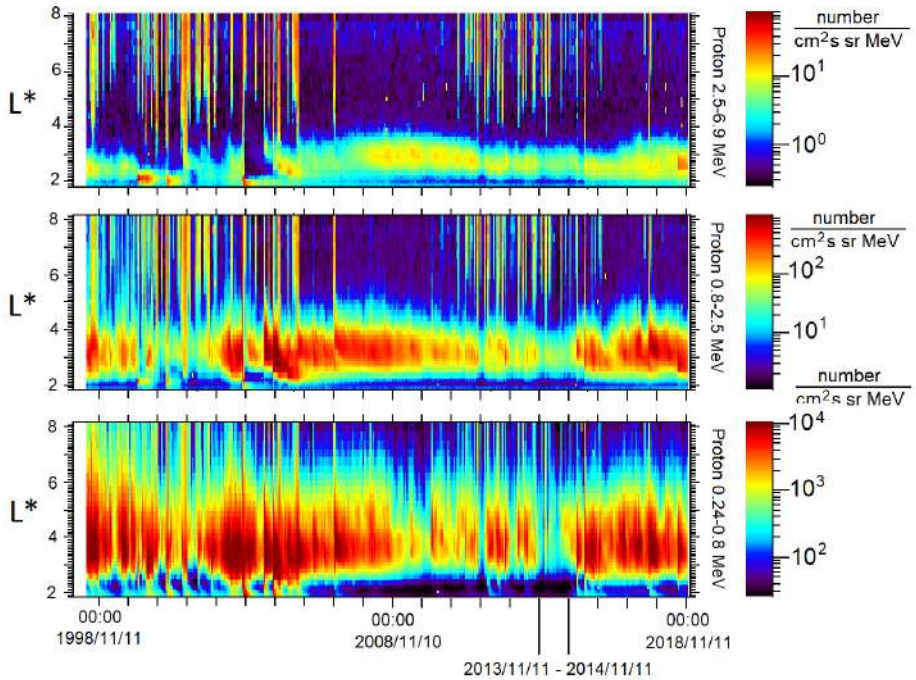

Figure 9: L-time cartographies of unidirectional proton flux measured by NPOES-15/SEM2 for several energies: 0.24-0.8 MeV (at the bottom), 0.8-2.5 MeV (in the middle) and 2.5-6.9 MeV (at the top), [19]. L^* is the radius (in Earth radii) of a particle's drift around the Earth if the magnetic field adiabatically relaxed to a dipole configuration. The graph shows flux drop in the bottom and middle panes around 2013/11/ – 2014/11/.

The mid-2014 – early 2015 was marked by never-before-seen undulations in cosmic ray intensity shown in Figure 7, they must have been related to: 1) the only observed space hurricane detected on 2014/8/20, [16]; 2) the mid-2014 jump in the rate of temperature increase in Figure 1. Cosmic rays are known to exhibit 27-day variability attributed to the solar synodic period; but never has the 27-day variability been as clear and well-pronounced as in 2014/6/20−2015/2/13. Figure 7 points to the Moon as a significant contributor to the undulations; since the only known source of energetic particles that could be influenced by the Moon is the Van Allen Belts, we must conclude that the undulations involved not just cosmic rays but also energetic particles from the Van Allen Belts. The tidal force produced by the synchronization of Full Moon and perigee must have "shaken" the Van Allen Belts hurling energetic particles into the Earth's atmosphere. The anatomy of the "shaking" is similar to that of magnetopause shadowing, when a solar emission, such as a gust of solar wind or a solar flare, temporarily changes the shape of the radiation belt interfering with the particles' typical drift around magnetic lines and forcing particles in all directions; the only difference is that the tidal force replaces solar emissions and is applied periodically. With the Van Allen Belts hurling energetic particles towards Earth, we may expect the number of particles in the Van Allen Belts to drop around the time of the undulations. Indeed, Figure 8 shows that the high-energy electron flux drastically dropped around the time of the undulations, the mid-point of the drop falls on 2017/7/; Figure 9 shows that the proton flux also decreased around 2013/11/ – 2014/11/, the mid-point falls on 2014/6/. Although 27-day variability is easily seen in Figure 8, it is especially well-pronounced during 2014/8/ – 2015/5/ in the top four rows. Recently considered 2014/8/25 – 2014/10/4 subperiod of the undulations was shown to comprise three stages corresponding to intervals of increase/decrease in Figure 7: 1) 2014/8/27 – 2014/9/7, similar to HILDCAA; 2) 2014/9/13-20 with low flux of high energy electrons; and 3) 2014/9/22 – 2014/10/2, also similar to HILDCAA, [17].

Recent work suggests that during extreme depletion of plasma density in the Van Allen Belts, some particles may be accelerated to ultra-relativistic energies, [20, 21]; even a small jet of such particles entering Earth's atmosphere can produce lumps of highly-energetic secondary particles perceived by people as UFOs, which would explain almost daily encounters of US Navy pilots with undetermined aerial objects high in the skies over the East Coast from the summer of 2014 to March 2015 reported by the US Defense Department, [22]. Figure 10 shows monthly and annual

UFO sightings, they were considerably above average in 2011 – 2016, reaching the all-time high at the time of the undulations in 2014/7/. As Figure 11 shows, the 1960 – 2010 portions of the graphs of UFO sightings and the speed of the magnetic North Pole are remarkably similar; the graphs differ in 2010 – 2016 due to the synchronization of Full Moon and perigee. Figure 12 shows a remarkable correlation between monthly UFO sightings and the bottom part of Figure 9 around 2010 – 2016.

Since energetic particles in the Earth's atmosphere are expected to increase the latter's temperature, we may expect a good correlation between the UFO sightings and temperature. Indeed, Figure 13 shows a remarkable similarity between the graph of the annual global UFO sightings in 1995/1/ – 1921/4/ and that of temperature anomalies in 1996/3/ – 2019/12/; the similarity of the two graphs suggests that such energetic particles affect Earth's temperature and are the main cause of current global warming. Even though pre-1995 UFO data contains too few sightings, Figure 14 reveals some similarity between the graphs of the annual global UFO sightings and temperature anomalies in 1960/1/1 – 1994/9/1; pre-1960 data is too sparse and potty to be of any use. Unfortunately, the post-2018 UFO data is likely to be corrupted by Starlink satellites reported by some as UFOs; so it is hard to make any future forecasts based on UFO sightings. Figure 13 suggests that global temperature will go down for several years; what happens afterward depends on whether the 2020/3/ maximum in UFO sightings is a true maximum or a result of reports of Starlink satellites.

The correlation of global temperature in 1900 – 2010 with the speed of the magnetic North Pole and the magnetic South Pole's rather sloth-like movement suggest that the largest temperature increase should be expected in the area around the two northern maxima of the total intensity of the Earth's magnetic field defined in Figure 4 and/or magnetic North Pole, Figure 15 shows that it is indeed so, and the highest temperature increases are between the two northern maxima of the total intensity of the Earth's magnetic field; the very highest increase is right in front of the magnetic North Pole. While the parameters in Figures 15 were chosen by NASA to dramatize the effects of global warming, Figure 16 provides a somewhat more balanced view; it shows that the two northern maxima of the total intensity of the Earth's magnetic field built two patches of increased temperature near them by 2009, in 2009 – 2012 a nexus developed between the patches along the path of the magnetic North Pole, by 2016 the nexus had widened to create a single large

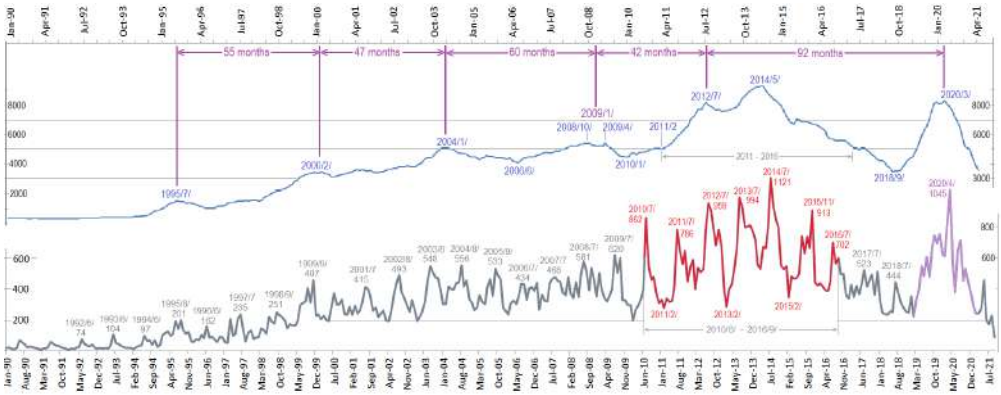

Figure 10: The bottom graph shows monthly global UFO sightings reported in 1990 – 2020, [23]. The top graph shows annual global sighting, the value at each month is calculated by adding the number of sightings in the month, in the preceding 6 months, and in the following 5 months. Pre-1995 counts are mostly in two digits and present too little information to be meaningful. Past-2018 data is likely to be corrupted by Starlink satellites.

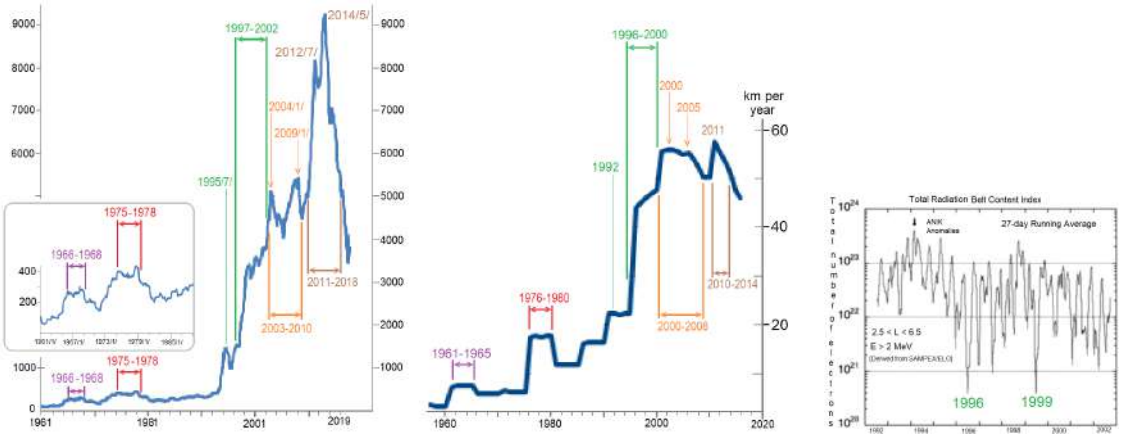

Figure 11: The left graph shows the annual global UFO sightings for 1961 – 2020, [23], the inset zooms in on the 1961 – 1990 period; the middle graph shows the speed of the magnetic North Pole, [4]. The graphs are not identical but exhibit very similar overall behavior, similar features are emphasized with similarly-colored labels. UFO sightings increased much more in 2011 – 2016 than in 2003 – 2010 even though the speed of the magnetic North Pole in 2010 – 2014 was comparable to the speed of the magnetic North Pole in 1999 – 2008; the additional increase in UFO sightings in 2011 – 2016 is due to the synchronization of Full Moon and perigee in 2010 – 2016. The right graph shows the total Radiation Belt Content index for the period 1992 – 2000 (monthly smoothing), [24]. Two drastic drop-downs occurred in 1996 and 1999, right at the time of the two drastic increases in the magnetic North Pole's speed. The 1975 – 1978 surge in UFO sightings encompassed the Petrozavodsk phenomenon.

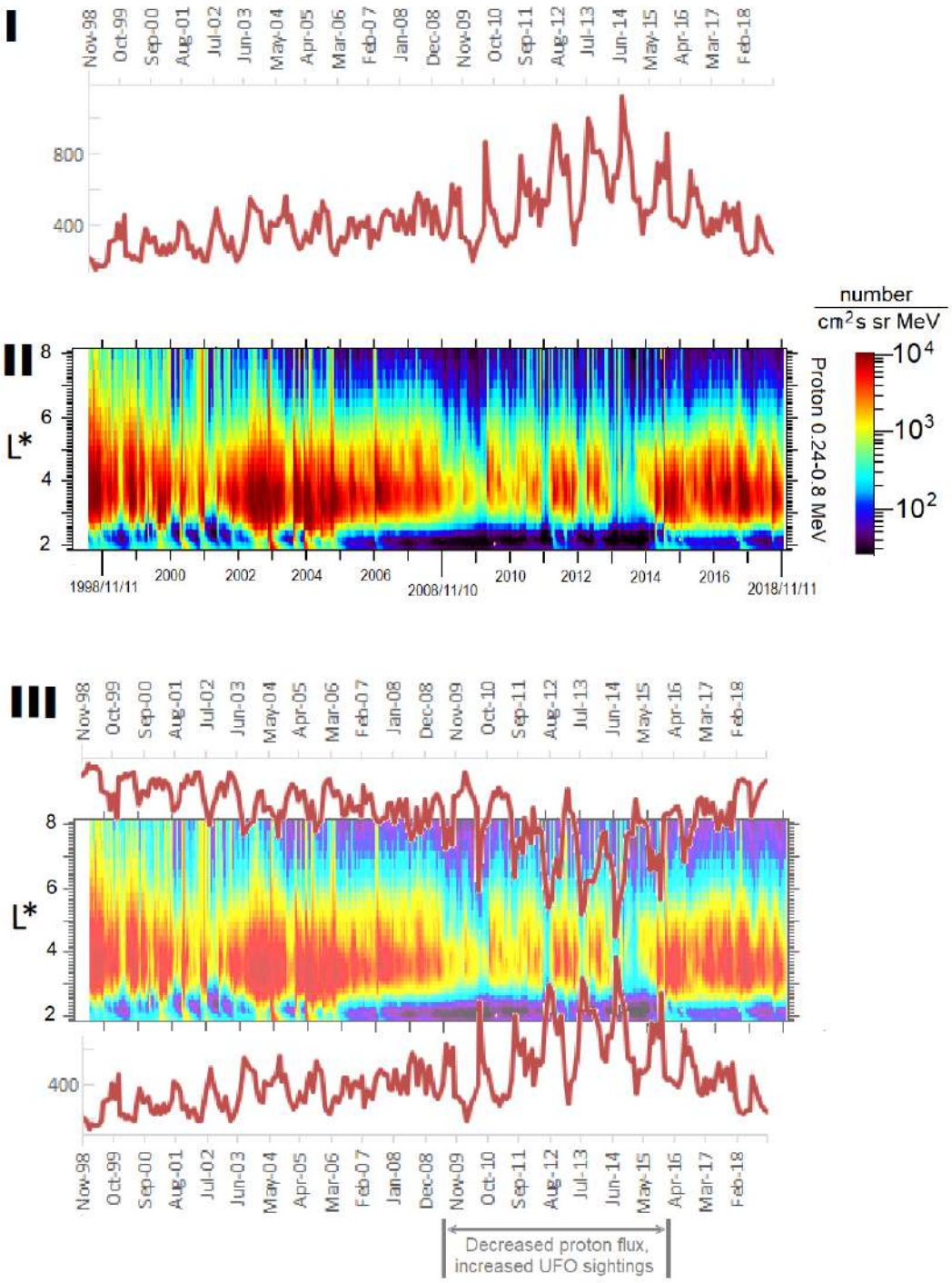

Figure 12: Frame I shows monthly UFO sightings from Figure 10, frame II shows the bottom part of Figure 9. In frame III, graph from frame I and its inversion are superimposed on frame II with $\approx$ 6.5-month lag. UFO sightings mirror proton flux: the maxima in UFO sightings more-or-less coincide with the gaps between maxima in proton flux; that is especially well-pronounced in 2010 – 2016. The highest number of UFO sightings correspond to extremely low proton flux for L$<$ 2.5.

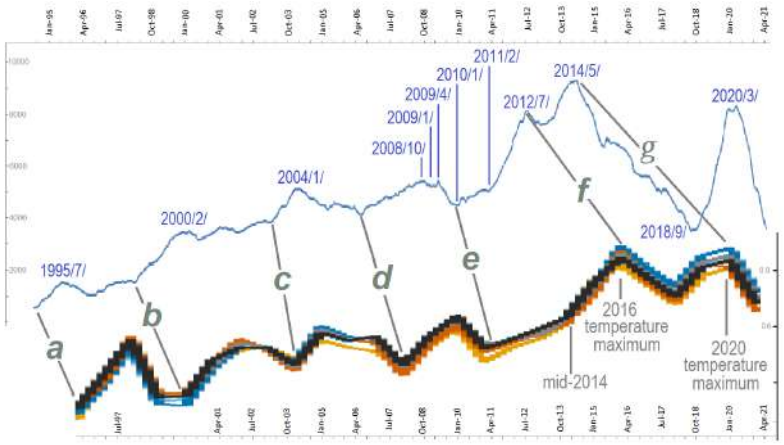

Figure 13: The top graph is the 1995/1/ – 1921/4/ annual global UFO sightings from Figure 10; the bottom graph is the 1996/3/ – 2019/12/ portion of Figure 1. The gray lines a - g divide both graphs into similar parts; the parts of the two graphs between each pair of consecutive gray lines are quite similar suggesting that the processes described by the two graphs are related. Lines *e* and *f* enclose both the largest uninterrupted temperature increase in the bottom graph and the largest uninterrupted increase in annual UFO sightings in the top graph. The 2014 and 2020 temperature maxima correspond to the 2012/7/ and 2014/5/ UFO maxima. The 2020 temperature maximum was only a few months after the first detection of Covid19.

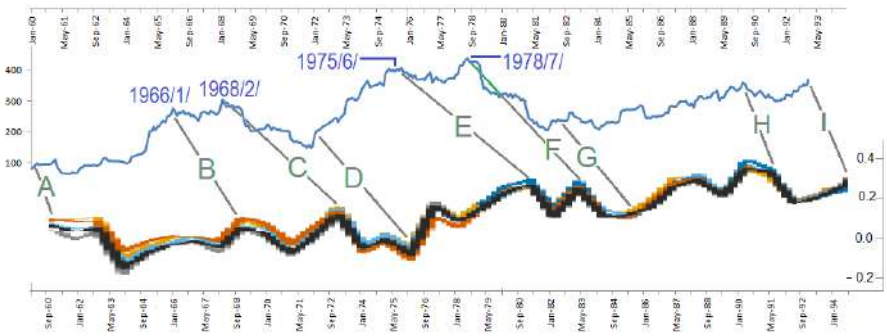

Figure 14: The top graph shows the annual global UFO sighting for 1960/1/ – 1993/1/ from Figure 10; the value at each month is calculated just like in Figure 13. The bottom graph is the 1960/9/ – 1994/9/ portion of Figure 1. Due to a rather small number of reported UFO sightings, the UFO graph does not properly reflect particle emissions from the Van Allen Belts, yet there is still some similarity between the graphs. The gray lines A - I divide both graphs into somewhat similar parts; the parts of the two graphs between each pair of consecutive gray lines are somewhat similar.

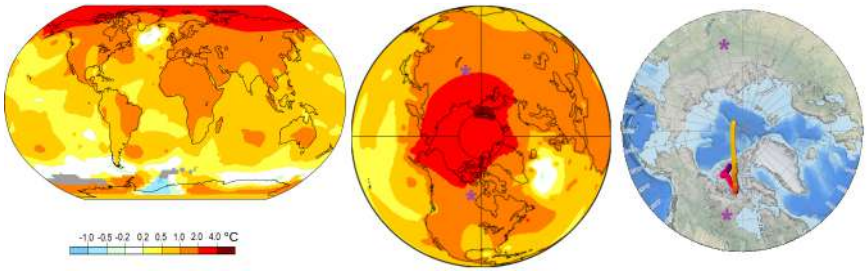

Figure 15: The left map shows NASA's average surface air temperatures increase in 2011 – 2021 compared to the 1956–1976 average; it indicates that the largest temperature increases have occurred in the Northern hemisphere; NASA chose 1956 – 1976 because it was the last minimum as Figure 1 shows. The middle map was generated using NASA's Scientific Visualization Studio generator with the same parameters as the top map, [25]. The modeled path of the magnetic North Pole in 1590 – 2022 is shown for reference only, [6]. The $\geqslant 2^{o}C$ temperature increase occurred around the two maxima of the total intensity of the Earth's magnetic field defined in Figure 4; the $\geqslant 4^{o}C$ temperature increase occurred close to the current magnetic North Pole's position. Purple asterisks mark approximate locations of the North-Eastern and North-Western maxima of the total intensity of the Earth's magnetic field in 2020.

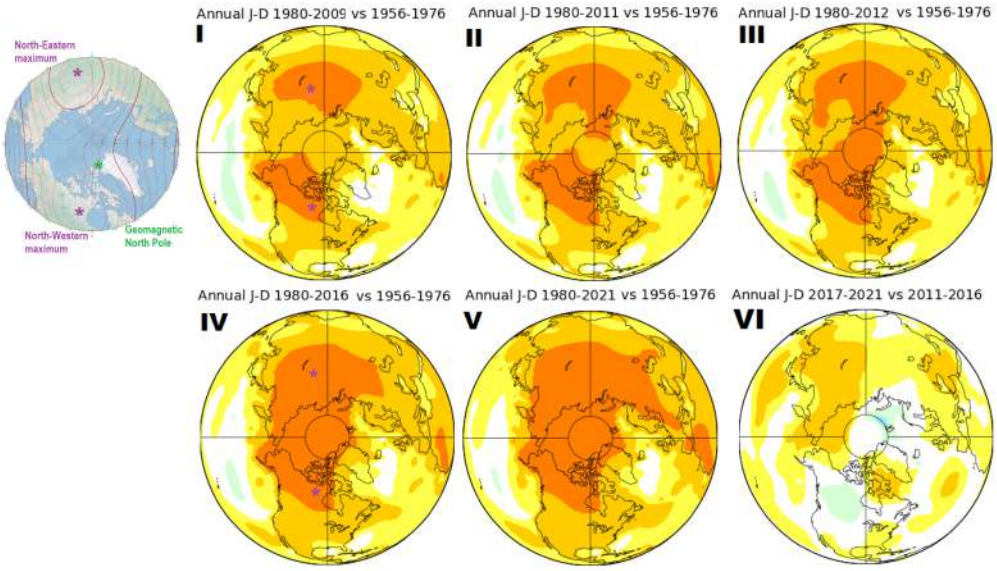

Figure 16: Evolution of the regions of $\geqslant 2^{o}C$ increase in the Northern hemisphere, generated using NASA's Scientific Visualization Studio generator using the same parameters as in Figure 15, [25]. On the left is a map of total intensity of the Earth's magnetic field from WWM-2015 with the maxima of the total intensity of the Earth's magnetic field in 2020 marked by purple asterisks, provided as a reference only. Frame I shows two patches of increased temperature that formed near the two northern maxima of the total intensity of the Earth's magnetic field defined in Figure 4 by 2009; frames II and III shows the growth of a nexus connecting the two patches along the path of the magnetic North Pole in 2009 – 2012; frame IV shows how the nexus had widened by 2016 to create a single spot of increased temperature; frame V shows the moving of increased temperatures towards Europe. To avoid possible misinterpretation, frame VI is included to show that there was no drastic temperature increase in 2017 – 2021; the only left-over holdout of increasing temperature is around the North-Eastern maximum.

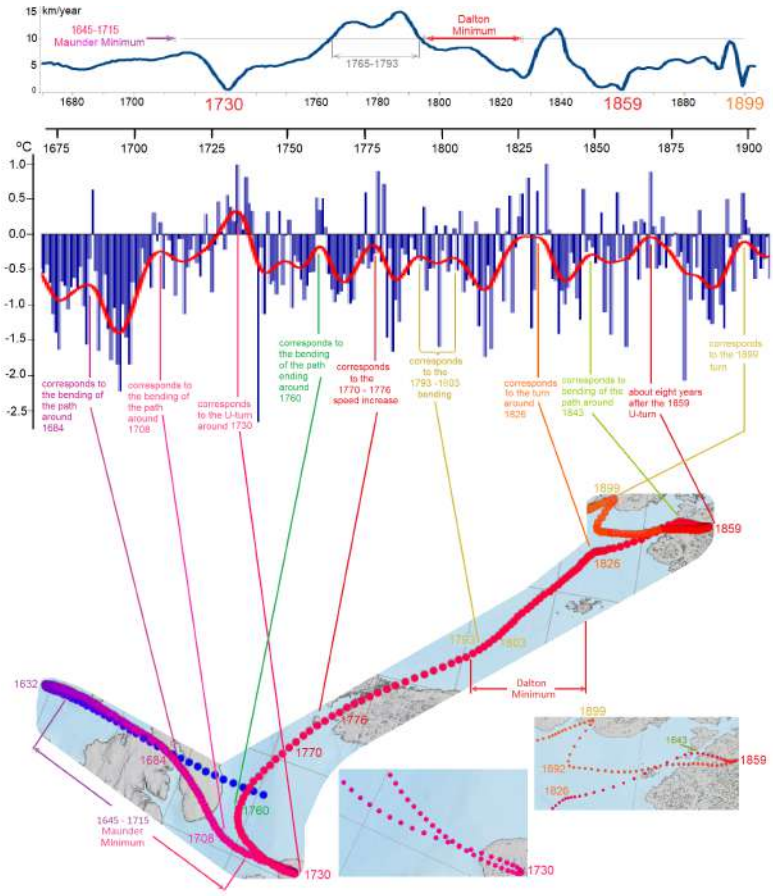

Figure 17: The top graph shows the speed of the magnetic North Pole. The middle graph shows mean Central England temperature annual anomalies in 1659 – 2010 in blue, its average in red, [2]. The bottom graph shows the Magnetic North Pole's path in 1590 – 1920, [6]; two insets zoom in on crowded portions of the graph. Pre-1900 speed of the magnetic North Pole was insignificant; temperature depended more on the path's curvature than the speed. The maxima of the red curve are matched with the turns of the path giving rise to them; although the matching is not perfect, it is sufficiently good to indicate the existence of a correlation between temperature and the movement of the magnetic North Pole. Colors carry no significance and are used solely for visualization.

Figure 18: Auroras observed during the Maunder Minimum, Schroeder, W., On the Existence of the 11-Year Cycle in Solar and Auroral Activity before and during the so-called Maunder Minimum, *Journal of geomagnetism and geoelectricity*, 1992 vol. 44 issue 2 pp.119-128, `https://www.jstage.jst.go.jp/article/jgg1949/44/2/44_2_119/_article`. Shown on the magnetic North Pole's modeled path are the numbers of auroras for each year with $\geqslant 3$ auroras.

spot that extended to Europe by 2021. Figures 15, 16 illustrate how inextricably linked are the increasing temperature and the Earth's magnetic field.

Mean Central England temperature annual anomalies is the longest record of instrument measurements of temperature going back to 1659. The speed of the magnetic North Pole in 1659 – 1900 was too insignificant to affect temperature; in the absence of significant speed, curvature of the path of the magnetic North Pole seems to correlated with temperature, as Figure 17 shows. The Maunder and Dalton minima coincided with the portions of the magnetic North Pole's path with low speed and low curvature.

Even though we have connected temperature variations to the Earth's magnetic field, the latter itself is a mere reflection of solar activity for 1) the 1632 U-turn was contemporaneous with drastically increased auroras as shown in Figure 18; 2) the 1730 and 1859 U-turns were contemporaneous with the Boston solar flare on 1730/10/22 and Carrington solar flare on 1859/9/1-2; 3) the Maunder and Dalton Minima coincided with the portions of the path with low speed and low curvature; 4) the 1950 increase in the speed of the Earth's magnetic field was amidst a host of solar flares and followed the alignment of planets in Figure 6 that was bound to increase solar emissions.

Figure 19 reveals that even powerful seismic activity in 1900 – 2015 seems to have followed the same pattern as global temperature and the speed of the magnetic North Pole.

With an increased number of aforementioned lumps of secondary energetic particles perceived as UFOs, one may expect an increased number of airplane accidents. Indeed, 2013/11/29 – 2015/10/31 saw an unusually large number of commercial airplane accidents, those widely discussed in media are shown in Table 2, 960 people died in merely 701 days of 2013/11/29 – 2015/10/31. There was also a large number of close calls reported by crews of commercial airplanes, [26]. Eerie circumstances of one of the accidents are illustrated in Figure 20. Those who find the connection of airplane accidents to energetic particles far-fetched, should be reminded that the 1996/7/17 explosion of TWA 800 was preceded by a streak of light of unknown origin. The 1996 – 2002 airplane crashes were contemporaneous with the 1006 – 2000 increase in the speed of the magnetic North Pole and 1996 – 2002 increase in the annual UFO sightings.

Figure 1 shows low temperature during 1907 – 1911, likely due to a diminished contribution of energetic particles from the Van Allen Belts. We may speculate that, for whatever reason, the

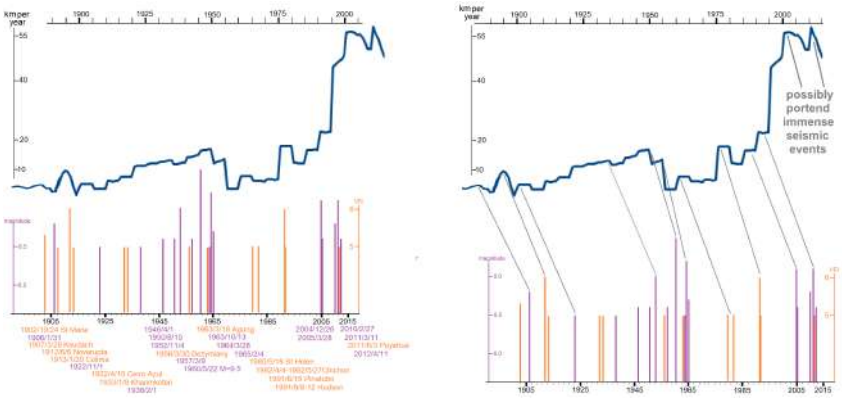

Figure 19: In the left pane, the speed of the magnetic North Pole is compared to the magnitude $\geqslant$ 8.5 earthquakes, shown in purple, and VEI $\geqslant 6$ eruptions, shown in orange, in $1900-2015$, [9, 14]. VEI=6 eruptions and magnitude $\geqslant 9.0$ earthquakes are represented by lines of the same height as the frequency of both is about the same; there were five VEI $\geqslant 5$ eruptions and four magnitude $\geqslant 9.0$ earthquakes in $1900-2021$. The right frame shows the same graphs but with the time scales synchronized, gray lines connect powerful seismic events with the corresponding increases in the speed of the magnetic North Pole. The two graphs move in tandem in $\approx 1900-1996$, with seismic activity;each surge in the speed of the magnetic North Pole corresponds to a cluster of 1 - 3 seismic events ≈ 15 years later. The post-1996 high values of the magnetic North Pole's speed have no corresponding seismic events as if portending upcoming seismic events of immense proportions.

energetic particles at the time did not enter the Earth's atmosphere in the usual way but instead as a large lump causing the Tunguska explosion. The proximity of the Tunguska explosion to the North-Eastern maximum of the total intensity of the Earth's magnetic field speaks in favor of the hypothesis.

§1 Concluding remarks.

The current global warming has been attributed to increased levels of CO_2; yet, the graphs of temperature and CO_2 bear no resemblance. In $1900-2010$ global temperature practically mirrored the behavior of the speed of the magnetic North Pole, powerful seismic activity, while the areas most affected by global warming were near the two northern maxima of the total intensity of the Earth's magnetic field and the magnetic North Pole. In $2010-2016$ global temperature and UFO sightings were also influenced by tidal forces whose contribution superseded that of the Earth's magnetic field. The demonstrated correlation between global temperature, movement of the magnetic North Pole and UFO sightings cannot be explained by increased levels of CO_2 but

Date & deaths		Airline, flight number, and a comment
		NO SUCH ACCIDENTS IN 2017– 2021
2016/5/19	66	EgyptAir 804, undetermined cause with evidence of fire onboard
2015/10/31	224	Metrojet 9268, undetermined cause, but blamed terrorists
2015/3/24	150	Germanwings 9525, attributed to co-pilot's suicide
2014/12/27	162	AirAsia 8501, captain removed breaker to cut power
2014/7/24	116	Air Algerie 5017, an obstruction of pressure sensors
2014/7/23	48	TransAsia Airways 222, unusual sounds before the crash, blamed on the crew
2014/3/7	227	Malaysia Airlines 370, just vanished
2013/11/29	33	LAM Mozambique Airline 470, attributed to pilot's suicide
2009/6/1	228	Air France 447, attributed to the crew's mistakes
2005/10/25	117	Bellview Airlines 210, undetermined cause
2002/5/25	225	China Airlines 611, attributed to fatigue cracking
2000/1/10	10	Crossair 498, attributed to pilot's incapacitation
1999/10/31	217	EgyptAir 990, attributed to pilot's suicide
1998/9/2	229	Swissair 111, onboard fire of unknown origin
1997/12/19	104	SilkAir 185, attributed to captain's suicide
1996/7/17	230	TWA 800, an explosion of a fuel tank following a hit by a streak or flash of light of unknown origin
		NO SUCH ACCIDENTS IN 1990 – 1995

Table 2: Unexplained, or incompletely explained civilian airplane accidents in 1990 – 2021 much discussed in mass media, [27]. The six crashes in the 16 months of 2013/11/29 – 2015/3/24, average a crash every 3 months. Never before or after so many commercial airplanes crashed in such a short time. There were two accidents within 24 hours in July 2014, the unusual circumstances of one of them are discussed in Figure 20. Each accident may be googled for more information. Dates are linked to Aviation Safety Network, airlines with flight numbers are linked to Wikipedia articles.

Figure 20: The right pane shows the crash site of Air Algeirie 5017 on 2014/7/24, [28]. The left pane shows magnitude $\geqslant 4$ earthquakes from 2014/7/21 22:00 UTC to 2014/7/30 1:00 UTC in $15^{\circ}S - 40^{\circ}N, 44^{\circ}W - 39^{\circ}E$, [9]. Quakes marked by the same color struck within 9.25 hours of each other, which we may consider being almost simultaneous. The line connecting one quake marked purple with the point between the other two, the line connecting the quakes marked pink, and the line connecting the quakes marked blue intersect at the same point, which is very close to the crash site of Air Algeirie 5017. The straight lines, of course, represent great circles on the globe. The three lines look like a giant reticle pointing at the Air Algeirie 5017 crash site. The middle pane zooms in on the intersection point to demonstrate how close it is to the crash site. This is an example of a rare phenomenon of the *seismic cross hairs*, its anatomy is to be discussed elsewhere.

can be explained by our hypothesis.

Truly bewildering is the currently popular view that different geophysical phenomena such as earthquakes and eruptions, movement of the magnetic poles, auroras, etc. are unrelated to each other; hardly can be attributed to a mere coincidence the concomitance of 1) an unusually high frequency of unexplained or incompletely-explained airplane accidents in $2013/11/29 - 2015/10/31$ illustrated by Table 2; 2) almost daily encounters of US Navy pilots with undetermined aerial objects from the summer of 2014 to March 2015, [22]; 3) the all-time high of UFO sightings in the middle of 2014 in Figure 10; 4) unusual and never-before-seen undulations of Figure 7; 5) the only known case of a space hurricane detected on $2014/8/20$, [16]; 6) depletion of the Van Allen Belts around 2014 illustrated by Figures 8, 9; 7) a sudden jump in the derivative of global temperature in mid-2014 exhibited in Figure 1. Already in 1923 in his book *New Lands*, Charles Fort suggested that so-called UFOs were coming from near-terrestrial space; while in 1950s, Dr J. Allen Hynek suggested that the so-called UFOs are likely to be a natural phenomenon. It is quite likely that some, if not all, airplane accidents of Table 2 were caused by lumps of highly-energetic secondary particles perceived by people as UFOs; had proper research been done, the disasters might have been mitigated.

References

[1] Global temperature, https://public.wmo.int/en/media/press-release/state-of-climate-2021-extreme-events-and-major-impacts, https://climate.metoffice.cloud/temperature.html. An interactive graph available at https://ourworldindata.org/co2-and-other-greenhouse-gas-emissions. 2

[2] Mean Central England Temperature, https://www.metoffice.gov.uk/hadobs/hadcet/, https://www.metoffice.gov.uk/hadobs/hadcet/cet_info_mean.html, based on Parker et al (1992), https://www.metoffice.gov.uk/hadobs/hadcet/Parker_etalIJOC1992_dailyCET.pdf. Numerical dataset https://www.metoffice.gov.uk/hadobs/hadcet/cetml1659on.dat. 3, 16

[3] NASA, https://en.wikibooks.org/wiki/High_School_Earth_Science/Climate_Change#/media/File:Instrumental_Temperature_Record_(NASA).svg 3

[4] Williams, B., The Correlation of North Magnetic Dip Pole Motion and Seismic Activity, *Journal of Geology and Geophysics*, 2016, https://www.longdom.org/open-access/the-correlation-of-north-magnetic-dip-pole-motion-and-seismic-activity-2381-8719-1000262.pdf, data from https://www.ngdc.noaa.gov/geomag/data/poles/NP.xy. The graph was kindly emailed to the author of the paper on 2021/1/1. 3, 7, 12

[5] NOAA: maps https://www.ngdc.noaa.gov/geomag/magfield-wist/, database https://www.ngdc.noaa.gov/geomag/calculators/magcalc.shtml#igrfgrid. 3, 5

[6] NOAA, Modelled magnetic poles' paths,https://www.ncei.noaa.gov/maps/historical_declination/. Proper boxes need to be checked. 5, 15, 16

[7] NASA's Solar Ssytem calculator, https://www.fourmilab.ch/cgi-bin/Solar. 6

[8] Jupiter syzygies. For 2002 – 2021 http://iaaras.ru/media/data/ae2021/ae_d4e.txt with the year appropriately selected; for 1991 – 2021 https://www.planetary.org/articles/06031044-oppositions-conjunctions-rpx; for 1990 – 2021 *Astronomical Phenomena for the Year 2021* with 2021 replaced by the required year; for 1912 – 1989 *Observer's handbook 1989* at https://www.rasc.ca/sites/default/files/publications/ObserversHandbook-1989.pdf with 1989 replaced by the required year from. Non-scientific http://www.astrology.com.pl/transits/2021/ with 2021 replaced by the appropriate year might be the most convenient to use. 7

[9] USGS earthquake catalog https://earthquake.usgs.gov/earthquakes/search/ and NOAA earthquake database https://www.ngdc.noaa.gov/hazel/view/hazards/earthquake/search. 6, 7, 8, 18, 19

[10] Space Weather Archives, http://www.solarstorms.org/SRefStorms.html. 6

[11] Lunar events http://astropixels.com/ephemeris/moon/moonnodes2001.html and https://www.fourmilab.ch/earthview/pacalc.html 7, 8

[12] Moscow Neutron Monitor http://cr0.izmiran.ru/mosc/main.htm, Oulu Neutron Monitor https://cosmicrays.oulu.fi/. Other monitors and data https://www.nmdb.eu/nest/, http://neutronm.bartol.udel.edu/. 8

[13] Yulbarisov, R.F., Galikyan, N.G., Mayorov, A.G. et al. Amplitude and Temporal Characteristics of 27-Day Variations in the Galactic Cosmic Ray Flux, Measured during the PAMELA Experiment between 2006 and 2016. Bull. Russ. Acad. Sci. Phys. 85, 1272–1275 (2021). https://doi.org/10.3103/S1062873821110381. 8

[14] Eruptions databases, https://www.ngdc.noaa.gov/hazel/view/hazards/volcano/event-search, https://volcano.si.edu/search_eruption.cfm. 7, 18

[15] Van Allen Belts in 2012, https://www.science.org/doi/10.1126/science.1233518, https://www.scientificamerican.com/article/third-van-allen-radiation-belt-makes-appearance-around-earth/ 7

[16] Qing-He Zhang et al, A space hurricane over the Earth's polar ionosphere, *Nature Communications*, vol. 12, article number: 1207 (2021), https://www.nature.com/articles/s41467-021-21459-y. 7, 10, 20

[17] Jaynes, A. N., et al. (2015), Source and seed populations for relativistic electrons: Their roles in radiation belt changes, J. Geophys. Res. Space Physics, 120, pp. 7240– 7254, https://agupubs.onlinelibrary.wiley.com/doi/10.1002/2015JA021234. The protion quoted is under Figure 4. 10

[18] D. L. Turner, T. P. O'Brien, J. F. Fennell, S. G. Claudepierre, J. B. Blake, A. N. Jaynes, D. N. Baker, S. Kanekal, M. Gkioulidou, M. G. Henderson, G. D. Reeves, Investigating the source of near-relativistic and relativistic electrons in Earth's inner radiation belt, *GJR Space Physics,* vol. 122, issue1, 2017, pp. 695-710, https://agupubs.onlinelibrary.wiley.com/doi/full/10.1002/2016JA023600. Similar graphs at https://angeo.copernicus.org/preprints/angeo-2018-98/angeo-2018-98.pdf, https://agupubs.onlinelibrary.wiley.com/doi/full/10.1029/2018JA025277. 9

[19] Sicard, A., Bourdarie, S., Lazaro, D., Standarovski, D., Ecoffet, R., et al. A new model for the 1-10 MeV proton fluxes (part of ONERA GREEN-V3 model). European Conference on Radiation and its Effects on Components and Systems (RADECS) 2019, Montpellier, France. https://hal.archives-ouvertes.fr/hal-02797017/document 9

[20] Allison, H., Shprits, Yu., Local heating of radiation belt electrons to ultra-relativistic energies, *Nature Communications,* 2020; 11: 4533, https://www.ncbi.nlm.nih.gov/pmc/articles/PMC7483540/. 10

[21] Allison, H., Shprits, Yu., Zhelavskaya, I., Wang, D., Smirnov, A., Gyroresonant wave-particle interactions with chorus waves during extreme depletions of plasma density in the Van Allen radiation belts, *Science Advances*, 2021, Vol 7, Issue 5, https://www.science.org/doi/10.1126/sciadv.abc0380. 10

[22] *New York Times* https://www.nytimes.com/2019/05/26/us/politics/ufo-sightings-navy-pilots.html 10, 20

[23] UFO Reporting Center, http://www.nuforc.org/webreports/ndxevent.html. 12

[24] Baker, D.N., Erickson, P.J., Fennell, J.F. et al. Space Weather Effects in the Earth's Radiation Belts. Space Sci Rev 214, 17 (2018), Figure 29. https://link.springer.com/article/10.1007/s11214-017-0452-7 12

[25] NASA's Scientific Visualization Studio generator is at https://data.giss.nasa.gov/gistemp/maps/index_v4.html; the parameters are taken from https://en.wikipedia.org/wiki/Instrumental_temperature_record, https://commons.wikimedia.org/wiki/File:Change_in_Average_Temperature.svg. 15

[26] Nine confirmed close-call encounters with UFOs, a) https://www.thestar.com/news/canada/2016/11/14/porter-plane-in-near-miss-with-drone.html; b) https://www.theguardian.com/technology/2016/apr/28/heathrow-ba-plane-strike-not-a-drone-incident, c) http://www.denverpost.com/business/ci_27872975/denver-bound-icelandair-flight-from-reykjavik-hit-by; d) http://www.dailymail.co.uk/news/article-3034472/Hero-Loganair-pilot-pulls-plane-North-Sea-nosedive-just-SEVEN-SECONDS-spare.html?ITO=1490&ns_mchannel=rss&ns_campaign=1490; e) http://avherald.com/h?article=47d74074; f) 8 http://www.atsb.gov.au/media/4897226/AO-2014-052%20Final.pdf; g) http://www.huffingtonpost.com/2014/01/06/ufo-jet-airliner-near-miss-over-uk_n_4549399.html; h) http://www.dailymail.co.uk/news/article-2339139/Was-bird-A-Plane-Or-UFO--Chinese-passenger-jet-

hits-mysterious-object-26-000ft-lands-severely-dented-nose-cone.html, http://cayodagyo.blogspot.com/2013/06/some-possibilities-of-object-that-had.html; i) http://www.ibtimes.co.uk/ufo-plane-glasgow-scotland-463308#. 17

[27] Unexplained, or not completely explained civilian airplane accidents in 2013 – 2016 much discussed in mass media. Aviation Safety Network https://aviation-safety.net/ and Wikipedia. Crashes at takeoff or landing, crashes of Boeing 747 Max, crashes of military planes like https://en.wikipedia.org/wiki/2016_Indian_Air_Force_An-32_disappearance, and crashes of small aircraft like https://www.cbc.ca/news/canada/calgary/tsb-report-jim-prentice-plane-crash-release-1.4635541 are not included in the table. 19

[28] Air Algeirie 5017, https://en.wikipedia.org/wiki/Air_Alg%C3%A9rie_Flight_5017 19